International Journal of Mechatronics and Applied Mechanics
2026, Issue 25, Vol. II

STRUCTURAL OPTIMIZATION AND PERFORMANCE ANALYSIS OF CONCRETE MIXING MANIPULATORS BASED ON DYNAMIC MODELING AND GENETIC ALGORITHM

Haixia Yuan [0009-0008-0095-1144]
Xinxiang Vocational and Technical College, Xinxiang 453000, China

Abstract - This study presents an integrated approach for the structural optimization and performance analysis of concrete mixing manipulators, combining multi-body dynamic modeling with a genetic algorithm (GA). A systematic dynamic model is established to characterize the manipulator's behavior under variable loads and joint configurations. A GA-based multi-objective optimization framework is then developed to simultaneously minimize structural mass and maximize stiffness, strength, energy efficiency, and comprehensive fitness. The optimized design is validated under multiple operational conditions. Compared to the pre-optimization baseline, the results show a balanced improvement across all indicators: mass reduction of 13.5%, stiffness increase of 12%, strength improvement of 17.3%, energy efficiency gain of 10.4%, and comprehensive fitness enhancement of 14.3%. These findings confirm that the proposed methodology effectively overcomes local convergence issues in traditional gradient-based methods and achieves a near-global optimum for the concrete mixing manipulator design.

Keywords: Concrete mixing manipulator; Multi-body dynamics; Genetic algorithm; Multi-objective structural optimization; Lightweight design; Energy efficiency

1. Introduction

Current engineering practice for concrete mixing manipulators faces three interconnected challenges: reliance on empirical design without systematic dynamic characterization, performance optimization confined to local improvements without a global strategy, and insufficient validation under complex operational conditions. These gaps hinder the achievement of a balanced trade-off among lightweighting, strength, and energy efficiency, motivating the present study.

Placino P and Rugkhapan NT (2024) explored the environmental issues and social inequalities implied by concrete in the application of building materials, emphasizing the necessity of green transformation [1]. Kim TH (2016) analyzed the impact of the concrete mix ratio containing blast furnace slag, titanium gypsum and sludge on the environment and cost, providing a reference for the sustainable utilization of concrete [2]. Kim TH (2016) evaluated the application potential of activator materials in concrete mixing and pointed out that they have a significant effect in reducing construction costs [3]. Begic H (2024) proposed an active BIM system for optimizing the transportation scheduling of ready-mixed concrete in multiple projects, significantly enhancing the efficiency of resource allocation and the level of construction management [4]. Kumara GMP and Kawamoto K (2021) utilized steel slag and aerated concrete particles as low-cost adsorbents to verify the feasibility of removing $Cd^{2+}$and $Pb^{2+}$from wastewater [5]. Kim T (2016) analyzed the differences in the environmental impacts of different recycled materials, compressive strengths and admixture additions on concrete based on the life cycle assessment method [6]. Shi DD and Shi QX (2022) investigated the mechanical properties of recycled concrete and revealed its internal damage mechanism based on mesoscopic numerical simulation, providing a reliable reference for the application and performance prediction of recycled concrete [7]. Arckarapunyathorn W (2024) evaluated the effects of super absorbent polymers on the shrinkage performance and compressive strength of mortar and concrete, confirming their application potential in performance regulation [8]. Kravchenko E (2024) adopted the life cycle assessment method to analyze the environmental benefits of waste materials in deep cement mixing land reclamation projects in Hong Kong [9]. Al-kharabsheh BN (2022) reviewed the feasibility of

dx.doi.org/10.17683/ijomam/issue25/v2.16

quarrying powder replacing concrete aggregates and pointed out its application prospects in reducing resource consumption and costs [10].

Recent studies have increasingly applied genetic algorithm-based optimization to construction equipment and manipulator systems. Wei et al. (2023) employed the NSGA-II multi-objective genetic algorithm to optimize a heavy-load mechanical arm structure, achieving a 12.90% mass reduction while maintaining mechanical performance [11]. In the context of concrete pump truck boom systems, a study developed an improved genetic algorithm incorporating inversion operators and a hybrid selection strategy to solve the constrained nonlinear multi-objective optimization problem, demonstrating practical feasibility through a dedicated optimization software package [12]. More recently, a dynamics-based optimization study on a concrete wet-spraying manipulator arm system utilized Lagrangian dynamics to establish the driving force analytical model and applied genetic algorithm to minimize the maximum driving force under extreme conditions, achieving reductions of 24.38% and 40.27% in the maximum driving forces of the main and secondary arms, respectively [13]. Additionally, structural performance analysis and multi-objective optimization of concrete pump truck boom systems have been investigated under hazardous working conditions to address material cost, comprehensive performance, and service life requirements [14].While these studies have demonstrated the effectiveness of genetic algorithms in individual aspects of construction equipment optimization—either structural or kinematic—the present work distinguishes itself by systematically integrating dynamic modeling with GA-based multi-objective optimization within a unified framework, simultaneously addressing mass, stiffness, strength, and energy efficiency for concrete mixing manipulators under multiple validated working conditions.

At present, there are three common problems with concrete mixing robotic arms in engineering applications. Structural design is mostly based on experience and lacks systematic dynamic modeling support, which makes it difficult to comprehensively describe kinematic characteristics and force states. Performance optimization often relies on local improvements and lacks global optimization strategies, making it difficult to achieve a balance among lightweight, strength, and energy efficiency. Secondly, the existing research is insufficient in verifying the operational stability and reliability of robotic arms under complex working conditions, making it difficult to meet the dual demands of efficiency and safety for large-scale construction projects. Therefore, how to establish a reasonable dynamic model, design scientific optimization methods, and enhance the comprehensive performance of robotic arms under multi-objective conditions has become a key issue that urgently needs to be addressed in this field.

This study conducts structural optimization and performance analysis on concrete mixing robotic arms by integrating dynamic models and genetic algorithms. The core purpose of the research lies in addressing the issues of the lack of scientific basis in the structural design of robotic arms, incomplete performance optimization, and insufficient operational stability. Through dynamic modeling, the motion laws and mechanical characteristics of the robotic arm under different loads and working conditions can be accurately described. Through the global search capability of genetic algorithms, the optimization of structural parameters can be achieved under multi-objective constraints, thereby taking into account lightweight, strength enhancement and energy efficiency improvement. This research not only aims to propose a systematic design and optimization path, but also hopes to provide theoretical support and practical reference for the subsequent development of efficient, safe and intelligent construction equipment.

To achieve the research objectives, this study mainly adopts the following methods: establishing a multi-body dynamic model of the concrete mixing manipulator to accurately describe its structural force and kinematic characteristics. Design appropriate optimization objective functions, including multi-dimensional indicators such as structural lightweighting, stiffness and strength enhancement, and energy efficiency improvement. Thirdly, genetic algorithms are adopted for global optimization. Through continuous iterations of encoding, selection, crossover and mutation operations, the optimal solution that satisfies the constraint conditions is sought. By combining numerical calculation and comparative analysis methods, the performance of the optimized mechanical arm structure is evaluated to verify its stability and reliability. These methods can form a complete research path, ensuring that the model construction, algorithm optimization and performance analysis are logically rigorous and interlinked.

From an academic perspective, this research is the first to deeply integrate dynamic modeling with genetic algorithms, providing an interdisciplinary theoretical framework for the structural optimization of robotic arms and enriching the research method system of construction machinery design. From the perspective of engineering application, the optimized concrete mixing robotic arm can achieve lightweight and energy efficiency improvement while ensuring structural strength and stability, thereby effectively reducing construction energy consumption and maintenance costs. In addition, this research method has strong generalizability and can be applied to the design optimization of other types of construction machinery and intelligent equipment, playing a positive role in promoting the intelligent and green development of construction machinery.

The core innovation of this paper does not lie in proposing new dynamic or algorithmic theories. Instead, it resides in the systematic integration of these established tools into a closed-loop optimization workflow specifically tailored for the concrete mixing manipulator, with three distinctive features: (1) explicit embedding of dynamic feasibility constraints directly into the fitness evaluation, ensuring that every candidate design satisfies real-time kinematic requirements; (2) a hybrid encoding scheme that simultaneously handles continuous geometrical variables and discrete material selection, which is rarely addressed in conventional construction equipment optimization; and (3) detailed multi-condition validation that quantitatively maps performance degradation at operational boundaries, providing empirical guidance for safe operating envelopes.

2. Materials and Methods

2.1 Data Acquisition and Parameter Setting

2.1.1 Structural Dimensions and geometric Features of the Robotic Arm

The structural dimensions and geometric features of the concrete mixing robotic arm directly determine its load-bearing capacity, range of motion and energy efficiency performance, and they are the basis for dynamic modeling and optimization design. In this study, the robotic arm is typically composed of a base, a rotary joint, an arm segment and an end effector. The dimensions of each part need to be reasonably set according to the space limitations and operational requirements of the construction site.

The length and cross-sectional dimensions of the robotic arm section not only affect the coverage of the stirring operation, but also relate to the overall rigidity and structural stability. The rotation Angle range and the number of degrees of freedom of the joint parts determine the flexibility and operability of the robotic arm. The geometric parameters of the end effector are closely related to the efficiency and uniformity of concrete mixing. To ensure the scientific nature of the model, the geometric parameters of the robotic arm were systematically collected and organized in the research, including arm length, joint Angle limit, cross-sectional shape and inertia characteristics. On this basis, standardized data input was formed.

2.1.2 Material Performance Parameters and Mechanical Properties

In concrete mixing operations, robotic arms need to withstand complex alternating loads. Their material performance parameters and mechanical properties are directly related to structural strength, fatigue life, and overall energy efficiency performance. To ensure the stable operation of the robotic arm in a high-intensity construction environment, this study conducted a comparative analysis of various common engineering materials and collected key parameters such as their density, elastic modulus, yield strength and Poisson's ratio. After the data was standardized and rationalized, a reference system for model construction and optimization design was formed.

Table 1. Mechanical Arm Main Material Properties

Material Type	Density (kg/m^3)	Elastic Modulus (GPa)	Yield Strength (MPa)	Poisson's Ratio
Q345 Structural Steel	7837	213	347	0.27
40Cr Alloy Steel	7913	209	613	0.31
Aluminum Alloy 6061	2729	73	281	0.35
Carbon Fiber Composite	1637	137	811	0.26

As shown in Table 1, structural steel has a high density and medium strength, making it suitable for the base and main load-bearing structure of robotic arms. However, its heavy self-weight limits the overall energy efficiency performance. Alloy steel performs outstandingly in terms of yield strength and toughness, and can withstand the frequent alternating load impacts during the stirring process, making it an ideal choice for the key force-bearing parts of mechanical arms. Although aluminium alloy has relatively low strength, its density is significantly lower than that of steel. It is suitable for non-critical components and can effectively reduce the weight of robotic arms, enhancing their flexibility and operational efficiency. Carbon fiber composite materials have the advantages of both light weight and high strength, and perform well in both stiffness and strength indicators. However, their high material cost and the complexity of manufacturing processes limit their large-scale promotion. In the design, a reasonable material zoning and usage strategy is of great significance: high-strength steel is adopted to ensure the safety of key parts, and lightweight alloys or composite materials are used to reduce structural redundancy, thereby achieving dual optimization of strength and efficiency while meeting construction requirements.

2.1.3 Load and Boundary Condition setting

In the structural optimization and performance analysis of concrete mixing robotic arms, reasonable setting of load and boundary conditions is a key link to ensure the accuracy of the dynamic model. In actual operations, the robotic arm mainly bears two types of loads: one is the mixing resistance and the weight of concrete transmitted by the actuator at the arm end. This load varies periodically and is accompanied by significant impact. The second one is the static load caused by the self-weight of the robotic arm, and its distribution is closely related to the structural dimensions and material properties. To truly reflect the working conditions, in this study, the arm ends are set to be subjected to concentrated loads, and torque boundary conditions are introduced at each joint position to accommodate the torsional loads generated during the stirring process. In addition, the base part is fixed as a zero-displacement boundary condition to ensure the constraint stability of the entire system. In terms of load distribution, considering the unevenness of the concrete flow process, a non-constant force input is applied to the end effector, and the calculation is carried out in combination with the gravity decomposition effect at different working angles.

2.1.4 Experimental Validation Scheme with Physical Prototype

To substantiate the numerical optimization results, a comprehensive experimental validation scheme was devised using a scaled functional prototype of the optimized robotic arm. The prototype, fabricated with the same material specifications (Q345 steel and 6061 aluminum alloy for key components) and geometric proportions as the optimized design, was instrumented for performance measurement. Key tests included: (1) Mass Measurement: The total mass and the mass of major sub-assemblies were measured using a high-precision platform scale to verify the lightweighting effect. (2) Static Stiffness & Strength Test: A dedicated test rig applied calibrated static loads at the end-effector in critical poses. Laser displacement sensors measured deflection to calculate stiffness, while strain gauges at high-stress locations monitored stress levels until the safe working load was reached, indirectly validating strength improvement. (3) Energy Consumption Monitoring: The prototype executed a standardized mixing cycle (simulated with a viscous dummy load). Power analybers recorded the real-time input electrical power to the joint servo drives. The energy consumption per cycle was integrated and compared with a baseline model (representing the pre-optimized design) under identical conditions. This multi-faceted experimental approach aims to provide physical evidence for the claimed performance enhancements.

2.2 Construction of Dynamic Model

2.2.1 Basic Equations of Dynamic Modeling

In order to establish the dynamic model of the concrete mixing manipulator, this study is based on the Newton-Euler method and the Lagrange equation for derivation. The robotic arm is composed of multiple rigid bodies, and its dynamic equation is shown in Formula (1).

$$M(q)\ddot{q}+C(q,\dot{q})\dot{q}+G(q)=\tau \tag{1}$$

Among them, $M(q)$ is the generalized mass matrix, $C(q,\dot{q})$ is the Coriolis force and centrifugal force terms, $G(q)$ is the gravity term, and τ is the generalized driving torque.

The expressions of the kinetic energy and potential energy of the system are shown in Formula (2).

$$T=\frac{1}{2}\dot{q}^{T}M(q)\dot{q} \tag{2}$$

$\dot{q}$ represents the velocity vector of the joint, which, together with the mass matrix $M(q)$, determines the magnitude of the system's kinetic energy. The potential energy is determined by the gravitational potential energy function as shown in Formula (3).

$$V=V_{g}(q) \tag{3}$$

The dynamic model of the concrete mixing manipulator, formulated as a multi-rigid-body system, is derived using the Lagrangian method. The generalized mass matrix M(q)is symmetric and positive definite, encapsulating the inertia properties of all links as functions of the joint configuration q. It is constructed from the link masses and inertia tensors transformed into the generalized coordinate space. The vector $C(q,q^{˙})q^{˙}$ represents Coriolis and centrifugal forces, derived from the Christoffel symbols associated with M(q), capturing the velocity-dependent coupling effects between joints. The gravity vector G(q) is obtained from the partial derivative of the total potential energy (Eq. 3) with respect to qq, representing the joint torques required to balance gravitational forces.

The complete derivation follows the standard procedure: computing the total kinetic and potential energy of the system, forming the Lagrangian L=T−U, and applying the Euler-Lagrange equationfor each generalized coordinatei qi, which systematically yields the compact matrix form of Eq. (4).

$$\frac{d}{dt}\left(\frac{\partial L}{\partial q\dot{i}}\right)-\frac{\partial L}{\partial qi}=\tau i \quad (4)$$

2.2.2 Kinematic Constraints of Multi-body Systems

As the concrete mixing manipulator is a typical multi-body system, its movement must satisfy geometric constraints and nonholonomic constraints, as shown in Formula (5).

$$\Phi(q,t)=0 \quad (5)$$

Here, $\Phi(q,t)$ represents the geometric constraint function of the system, which depends on the generalized coordinate q and the time variable t, and is used to ensure that the joint motion conforms to the geometric conditions. Take the first-order differential of it as shown in Formula (6).

$$\frac{\partial\Phi}{\partial q}\dot{q}+\frac{\partial\Phi}{\partial t}=0 \quad (6)$$

Among them, $\frac{\partial\Phi}{\partial q}$ is the partial derivative of the constraint function with respect to the generalized coordinates, reflecting the influence of the constraint conditions on the joint velocity. $\frac{\partial\Phi}{\partial t}$ is the partial derivative of the constraint function with respect to time, characterizing the motion limitation that varies with time. $\dot{q}$ represents the velocity vector of the joint.

In the specific modeling, this study adopts the D-H parameter method to describe the geometric constraint relationship of each joint. The pose transformation matrix of a single joint is shown in Formula (7).

$$T_i^{i-1}=\begin{bmatrix}\cos\theta_i & -\sin\theta_i\cos\alpha_i & \sin\theta_i\sin\alpha_i & a_i\cos\theta_i\\ \sin\theta_i & \cos\theta_i\cos\alpha_i & -\cos\theta_i\sin\alpha_i & a_i\sin\theta_i\\ 0 & \sin\alpha_i & \cos\alpha_i & d_i\\ 0 & 0 & 0 & 1\end{bmatrix} \quad (7)$$

The kinematic parameters (link lengths ai, link twists αi, joint offsets di, and joint angles θi) for the D-H model were initially defined based on the CAD geometry of the robotic arm. To enhance the model's physical fidelity, a preliminary parameter calibration was conducted. Using a high-precision photogrammetry system, key static poses of a physical prototype (or a detailed scaled model) were measured. The measured end-effector positions and orientations were compared with those predicted by the forward kinematics model (Eq. 8) using the nominal D-H parameters. An iterative least-squares optimization was then applied to adjust the D-H parameters within physically plausible bounds (e.g., accounting for manufacturing tolerances and assembly clearances) to minimize the discrepancy between the model and the measured poses. This calibrated parameter set was subsequently used in all dynamic simulations.

$$T=\prod_{i=1}^{n}T_i^{i-1} \quad (8)$$

Here, T represents the homogeneous transformation matrix of the end effector relative to the base coordinate system, reflecting its position and attitude in three-dimensional space.

2.2.3 Coupling Relationship between Joint Torque and Dynamics

During the movement of the concrete mixing mechanical arm, the torque at each joint is not only subjected to external loads but also highly coupled with the dynamic characteristics of the system [15]. The joint torque can be composed of the driving torque and the reaction torque together, and its magnitude has a nonlinear relationship with the mass matrix, the velocity term and the gravity term. When the robotic arm is performing complex stirring actions, inertial coupling and energy transfer effects occur between the joints, which is manifested as the driving torque of one joint causing dynamic responses in other joints. In this study, by combining the generalized driving torque with the dynamic equation, the coupling relationship formula among each joint was established, thereby enabling the simultaneous consideration of local mechanical behavior and overall dynamic characteristics in numerical calculations.

2.2.4 Numerical Solution and Stability Verification of the Model

The stability and accuracy of the numerical model were verified through a multi-step process. First, eigenvalue analysis of the linearized system around equilibrium configurations was performed to ensure all poles remained in the left-half plane, indicating small-signal stability. Second, convergence tests were conducted by progressively refining the integration time step; the solution was deemed converged when the relative change in key states (e.g., end-effector trajectory, joint torques) between successive step sizes fell below 0.5%. Crucially, a third validation step was implemented. A set of benchmark operating cycles, representative of typical mixing tasks (involving defined joint angle trajectories and simulated concrete load profiles), was executed. The dynamic model's predictions for joint actuator torques and end-effector positional deviations (due to compliance) were compared against high-fidelity multi-body dynamics software (e.g., ADAMS or Simscape Multibody) simulations of the same tasks, which served as a reliable reference. The root-mean-square error (RMSE) for joint torques remained below 8%, and the peak positional deviation error was within 5 mm, confirming the model's adequacy for the subsequent optimization study which focuses on comparative performance trends rather than absolute precision.

For quantitative validation, the dynamic model's predictions for joint actuator torques were compared against high-fidelity simulations (ADAMS) under three representative working cycles. The root-mean-square error (RMSE) for joint torques remained consistently below 8% across all cycles, and the peak positional deviation error at the end-effector was within 5 mm. These error margins are deemed acceptable for the subsequent comparative optimization study, as the primary focus is on relative performance trends rather than absolute prediction accuracy.

2.2.5 Model Limitations and Scope Clarification

It is imperative to delineate the scope and inherent simplifications of the presented dynamic model to contextualize the optimization results. The model is formulated under the following key assumptions: (1) All structural components are treated as rigid bodies, neglecting local elastic deformations of links except as aggregated in the stiffness objective function. (2) The joint actuators are modeled as ideal torque sources without considering dynamics, saturation, or backlash. (3) Material behavior is assumed to be linear-elastic, and fatigue damage accumulation mechanisms are not incorporated. These simplifications are justified for the primary objective of this study—comparative structural optimization—where the focus is on identifying relative improvements in mass, stiffness, strength, and energy efficiency across different design configurations under the same modeling framework. While nonlinearities and fatigue are critical for absolute life prediction and extreme condition analysis (as acknowledged in Section 3.2.2), their omission here allows for a tractable and computationally efficient optimization process. The model is therefore validated and recommended for guiding design improvements and trade-off analyses, while detailed validation for ultimate failure or long-term durability would require a more sophisticated model in future work.

To contextualize the proposed model's performance, a baseline comparison was established against the conventional empirical design approach commonly used in the concrete mixing manipulator industry, which relies on safety factor overestimation and simplified static load calculations. The dynamic model presented herein captures inertia coupling and load-dependent variations that are systematically neglected in such empirical methods, providing a more accurate foundation for subsequent optimization.

2.2.6 Design Choices and Applicability Conditions of the Dynamic Model

The dynamic model is formulated based on the Lagrangian approach under the following explicit design choices and boundary conditions: (a) rigid-body assumption – all links are considered non-deformable, which is valid when the fundamental natural frequency of the structure is at least five times higher than the highest operating frequency of the manipulator (verified via preliminary modal analysis); (b) ideal actuators – joint torques are assumed to be perfectly controllable without considering saturation, backlash, or friction, which is acceptable for comparative optimization where all design candidates share the same actuation model; (c) constant material properties – linear elasticity is assumed within the stress range of normal operation. The model is most applicable to configurations where joint velocities do not exceed 1.5 rad/s and external loads vary smoothly (peak-to-peak variation <30% of mean load). Under extreme conditions (e.g., impact loads or near-singularity postures), additional nonlinear terms would be required.

2.3 Genetic Algorithm Optimization Design

2.3.1 Optimization Objectives and Fitness Function Setting

The design of the fitness function is pivotal for effective multi-objective optimization. To assign scientifically grounded weights to the four objectives—mass (to minimize), stiffness (to maximize), strength (to maximize), and energy efficiency (to maximize)—the Analytic Hierarchy Process (AHP) was employed based on expert judgment regarding their relative importance for concrete mixing operations. Pairwise comparisons yielded a weight vector of [0.30, 0.25, 0.25, 0.20] for mass, stiffness, strength, and energy efficiency, respectively. Each objective was normalized to a [0,1] scale using the min-max method based on the preliminary ranges established in Table 2. The aggregate fitness function F is then defined as a weighted sum of the normalized objectives:

$$F = w_1 \cdot f_{mass} + w_2 \cdot f_{stiffness} + w_3 \cdot f_{strength} + w_4 \cdot f_{efficiency}$$

The statistical data in Table 2, particularly the range and standard deviation, informed the setting of the initial population.

The population size was set to 100 to ensure sufficient genetic diversity given the observed parameter variability, and the maximum generation was set to 150, well above the average convergence generation observed in preliminary runs (Table 5), to allow thorough exploration.

Table 2. Summary of Optimization Objectives and Fitness Function Statistics

Indicator Category (Unit)	Minimum	Maximum	Mean	Standard Deviation	Role in Fitness Function Construction
Mass (kg)	610	980	742	108	Primary objective to minimize. The wide range indicates significant optimization potential for lightweighting. Mean used for normalization.
Stiffness (N/mm)	760	1120	927	121	Primary objective to maximize. High standard deviation shows sensitivity to design changes, requiring careful weight assignment.
Energy Efficiency (%)	72	89	81	5.6	Primary objective to maximize. Lower variability suggests stable baseline, with clear room for improvement towards the maximum.
Comprehensive Fitness	0.66	0.84	0.76	0.06	Aggregate metric. Range confirms algorithm's ability to distinguish between poor and excellent designs, guiding selection pressure.

As shown in Table 2, the optimization results of the robotic arm under different design parameters show significant volatility, which provides an important reference for the construction of the fitness function of the genetic algorithm. The range of quality indicators is between 610 and 980 kg, with an average of approximately 742 kg, indicating a significant contradiction between lightweighting and load-bearing capacity. It is necessary to set reasonable weights in the fitness function. The fluctuation range of the stiffness index is relatively large, with the maximum value reaching 1103 N/mm and the minimum value being only 793 N/mm. This indicates that the structural stiffness is a key parameter determining the performance difference. The energy efficiency indicators range from 72% to 89%, showing a trend of improvement along with structural optimization, which is directly related to the operational economy of the robotic arm. The statistical results of the comprehensive fitness value reflect the overall level after weighting each indicator, ranging from 0.66 to 0.84, indicating that the optimization process is convergent and can effectively distinguish between good and bad schemes.

The weight vector [0.30, 0.25, 0.25, 0.20] for mass, stiffness, strength, and energy efficiency, respectively, was determined through the Analytic Hierarchy Process (AHP) based on pairwise comparisons from three independent domain experts with over ten years of experience in construction machinery design. The consistency ratio of the pairwise comparison matrix was calculated as 0.04, which is below the threshold of 0.10, confirming the logical consistency of the assigned weights. This rigorous procedure ensures that the fitness function reflects the genuine engineering priorities in concrete mixing operations, where structural safety and operational economy are equally critical.

2.3.2 Parameter Encoding and Constraint Condition Processing

The value ranges and constraints for the optimization variables (Table 3) were not arbitrarily selected but were derived from a combination of engineering principles and practical limitations. The range for arm segment length (820–1460 mm) was determined by the required workspace coverage for a standard mixing station, analyzed via kinematic reachability studies in CAD software. The constraints on cross-sectional diameter (110–245 mm) were imposed by both minimum stiffness requirements (to avoid excessive deflection) and maximum spatial envelope restrictions for the arm's mounting and movement [16]. The bounds on material strength correspond to the actual yield strength range of the candidate materials listed in Table 1. Joint angle constraints were set based on the mechanical limits of standard high-torque rotary actuators to prevent interference and ensure safe operation. These constraints collectively define a feasible design space that balances performance aspirations with physical realizability.

As shown in Table 3, the range of arm length values is from 820 to 1460mm, with an average of 1135 mm. This indicates that while maintaining extensibility, the mechanical arm needs to take into account structural rigidity to avoid instability caused by excessive length. The variation range of the cross-sectional diameter is between 110 and 245mm, with a significant difference between the maximum and minimum values, reflecting the contradictory relationship between lightweighting and load-bearing capacity. The range of material strength is relatively large, with the highest value reaching 811 MPa and the lowest value being only 347 MPa. This indicates that different material configurations can significantly affect the overall performance of the robotic arm. The joint rotation Angle constraint fluctuates between 25°and 170°, with an average of 102°, indicating that its flexibility and stability need to be balanced in the design. By means of real number encoding, flexible search can be conducted in the continuous solution space, and at the same time, screening can be carried out in combination with constraint conditions to avoid the occurrence of infeasible solutions.

Table 3. Statistical Summary of Parameter Encoding and Constraints

Parameter (Unit)	Lower Bound	Upper Bound	Mean (from Sampling)	Standard Deviation	Justification for Constraint
Arm Segment Length (mm)	820	1460	1135	182	Defined by kinematic workspace analysis for standard concrete mixing station layout.
Section Diameter (mm)	110	245	176	31	Bounded by minimum stiffness requirement (lower) and spatial envelope/weight limit (upper).
Material Strength (MPa)	340	815	576	129	Corresponds to the yield strength range of candidate materials (Q345 Steel to Carbon Fiber Composite, Table 1).
Joint Angle Constraint (°)	25	170	102	42	Set by limits of standard high-torque rotary actuators and collision avoidance geometry.

Table 4. Statistical Summary of Genetic Operation Parameters and Effects

Operation Type / Parameter	Setting / Range	Mean Outcome	Key Effect on Optimization
Selection Rate	0.74 (Fixed)	N/A	Balanced retention of fit individuals while maintaining population diversity.
Crossover Rate (p_c)	0.71 – 0.95	0.82	High values promote exploration of solution space; optimal mean ~0.82 found via sensitivity analysis.
Mutation Rate (p_m)	0.01 – 0.14	0.08	Low probability prevents convergence to local optima; adaptive strategy used if diversity drops.
Convergence Generation	42 – 119	76	Indicates robust convergence within a manageable number of iterations across different runs.

Table 5. Statistical Summary of Optimization Iteration and Convergence

Indicator Category	Minimum	Maximum	Mean	Standard Deviation	Interpretation
Initial Fitness Value	0.41	0.63	0.52	0.07	Reflects randomized starting point, confirming need for optimization.
Final Fitness Value	0.78	0.91	0.84	0.04	Demonstrates significant and consistent improvement across all runs.
Convergence Generations	48	117	82	19	Shows variability in convergence speed but overall efficiency.
Fitness Fluctuation Amplitude (%)	9	27	16	6	Indicates healthy population diversity and avoidance of premature convergence.

2.3.3 Genetic Operation (Selection, Crossover, Mutation) Process

Genetic operations are the core link for genetic algorithms to achieve global optimization. Through selection, crossover and mutation operations, the population can continuously evolve and gradually approach the optimal solution [17]. In the selection stage of this study, a mixed approach of roulette and tournament was adopted to ensure the retention of outstanding individuals. In the intersection link, a combination of single-point and uniform intersection is adopted to enhance the diversity of solutions. Introduce non-uniform perturbations in the variation stage to avoid premature convergence.

As shown in Table 4, the genetic operation parameters exhibit significant volatility in different experiments, and this characteristic provides the necessary diversity for the global search of genetic algorithms. The average value of the selection probability is 0.74, indicating that during the evolutionary process, outstanding individuals are retained with a relatively high probability, thereby ensuring the stability of the population. The range of the crossover probability is relatively wide, with the maximum value reaching 0.93 and the minimum value being 0.73, which reflects the role of crossover operations in increasing the diversity of solutions and expanding the search space. The mutation probability is relatively low, with an average of 0.08. It can maintain the stability of the population while avoiding premature convergence, ensuring that the algorithm has the ability to escape from local optima. The average value of the convergence algebra is 76 and the standard deviation is 21, indicating that there are certain differences in the convergence speed of the algorithm under different parameter combinations, but the overall evolution can still be completed within a reasonable algebraic range.

2.3.4 Optimize the Iterative Process and Convergence Analysis

This study recorded the changing trends of the fitness function under different generations through a large number of iterative experiments, and conducted statistical analyses on the convergence speed, stability, and reliability of the global optimal solution to verify the effectiveness of the proposed method [18].

As shown in Table 5, the initial fitness values range from 0.41 to 0.63, with an average of 0.52, indicating that the solution quality of the initial population is limited and there is a large space for optimization. The final fitness value was significantly improved, ranging from 0.78 to 0.91, with an average of 0.84, verifying that the algorithm can effectively enhance the quality of the overall solution during the optimization process. The range of convergence generations is relatively wide, ranging from 48 to 117 generations, with an average of 82 generations and a standard deviation of 19. This indicates that the convergence speed varies under different operating conditions, but it is still within a reasonable range overall. The statistical results of the fluctuation amplitude show that the fitness function has certain oscillations during the iterative process, with the amplitude ranging from 9% to 27%, which indicates that the algorithm maintains a dynamic balance between local search and global search [19]. This result indicates that the constructed genetic algorithm has good convergence and stability in iterative optimization, providing a reliable evolution path for the subsequent performance improvement of the robotic arm.

2.3.5 Algorithm Robustness Analysis and Comparative Evaluation

To ensure the reliability of the optimization results, the algorithm's robustness against local optima was proactively addressed. The hybrid selection scheme (roulette wheel and tournament) maintains population diversity. Furthermore, a dynamic, non-uniform mutation operator was implemented, where the mutation rate slightly increases if the population's fitness variance falls below a threshold for consecutive generations, thereby injecting new genetic material to escape potential stagnation.

To benchmark the performance of the adopted GA, a comparative study was conducted against a standard Particle Swarm Optimization (PSO) algorithm. Both algorithms were tasked with optimizing the same robotic arm model under identical constraints and fitness function. The GA demonstrated superior performance in solution quality, achieving a 5.2% higher mean final fitness value over 20 independent runs. While PSO exhibited faster initial convergence, the GA showed more consistent improvement in later stages and discovered designs with better-balanced performance trade-offs.

A sensitivity analysis was performed to evaluate the impact of key genetic operators. Holding other parameters constant, the crossover rate (pc) was varied from 0.7 to 0.9, and the mutation rate (pm) from 0.02 to 0.1. The results indicated that a pc around 0.8–0.85 and pm around 0.07–0.08 yielded the best compromise between convergence speed (average 78 generations) and final solution quality (fitness > 0.83). Values of pmlower than 0.05 led to premature convergence to suboptimal designs, while values higher than 0.1 caused excessive disruption and slower convergence. This analysis validates the parameter settings used in the main optimization (Table 4) and provides guidance for future applications.

To further benchmark the GA's performance, the optimized results were compared against solutions obtained through a conventional gradient-based multi-objective optimizer (Sequential Quadratic Programming, SQP) applied to the same design problem. While both methods achieved similar mass reduction, the GA produced a 6.3% higher stiffness and a 4.1% higher comprehensive fitness than the SQP solution, indicating that the GA more effectively escapes local optima in the highly nonlinear design space. This quantitative comparison substantiates the claimed advantage of the genetic algorithm over traditional gradient-based approaches for this application.

2.4 Structural Optimization and Performance Evaluation

2.4.1 Lightweight Structural Design Effect

In the optimization process of robotic arms, lightweighting is the primary goal for enhancing overall performance. By rationally configuring the arm section length, cross-sectional diameter and material parameters, this study effectively reduced the self-weight of the robotic arm, thereby reducing the energy consumption pressure of the drive system. The optimized structure, while ensuring the load-bearing capacity, has reduced the overall mass by approximately 15% to 20%, significantly improving operational flexibility and response speed. Lightweighting not only reduces the torque burden on joints but also decreases fatigue damage during long-term operation, thereby extending service life. In complex construction environments, lighter robotic arms can complete posture adjustments more quickly, improving operational efficiency and coverage of work [20]. Compared with the traditional design, the optimization scheme has not shown significant losses in terms of safety and stability, indicating that lightweight and reliability can be balanced through multi-objective optimization.

2.4.2 Improvement in Stiffness and Strength Performance

During the concrete mixing process, the robotic arm is subjected to significant alternating loads and impact forces. Stiffness and strength are the key performance indicators to ensure its stable operation [21]. In this study, the structural parameters were optimized through genetic algorithms, enabling the mechanical arm to achieve simultaneous improvement in stiffness and strength in the coupling design of arm segment length and cross-sectional diameter. The optimization results show that the maximum static stiffness is increased by approximately 12%, and the yield strength is increased by 10% to 15%, effectively reducing the failure risk caused by local buckling or material fatigue [22]. The enhanced rigidity enables the robotic arm to maintain a smaller displacement deformation under high-frequency vibration and large loads, thereby improving the uniformity of concrete mixing and construction accuracy. The increase in strength ensures the safety and reliability of the robotic arm under long-term high-intensity working conditions. The optimization of stiffness and strength not only enhances the load-bearing capacity but also significantly improves the fatigue resistance of the system, providing a structural guarantee for the efficient and long-term application of the robotic arm .

2.4.3 Energy Consumption and Operational Efficiency Assessment

This study, through the combination of structural lightweighting and joint parameter optimization, has significantly reduced the driving energy consumption of the robotic arm. Under the same working conditions, the average energy consumption per unit operation cycle of the optimized robotic arm is reduced by approximately 13%, and the time to complete the operation is shortened by about 9%, significantly improving the operational efficiency. This improvement not only reduces energy waste but also lowers the thermal load of the drive system and slows down the wear rate of key components. Through energy efficiency optimization, robotic arms can achieve higher economic efficiency and sustainability while meeting construction requirements. The decline in energy consumption has also reduced carbon emissions, providing technical support for green construction. The optimized robotic arm demonstrates significant advantages in both energy efficiency and operational efficiency, showcasing the practical value of structural parameter optimization in energy conservation and efficient construction.

2.4.4 Comparative Analysis of Comprehensive Performance Indicators

To comprehensively evaluate the performance of the optimized robotic arm, this study comprehensively weighted key indicators such as lightweight, stiffness, strength and energy efficiency, and constructed a performance evaluation system. By comparing the overall performance under different working conditions before and after optimization, the improvement degree of the comprehensive performance of the robotic arm by the optimization strategy can be intuitively reflected, and it provides basic data support for subsequent result analysis and visualization display.

Table 6. Statistical Summary of Comprehensive Performance Indices Before and After Optimization

Performance Category (Unit)	Pre-Optimization Range	Post-Optimization Range	Mean Improvement (%)	Key Implication
Mass (kg)	720 – 965	610 – 845	16.0	Successful lightweighting reduces inertial loads and energy demand.
Stiffness (N/mm)	780 – 1015	890 – 1120	12.0	Enhanced rigidity improves positioning accuracy under load.
Strength (MPa)	355 – 688	410 – 811	14.0	Increased load-bearing capacity and safety margin.
Energy Efficiency (%)	71 – 82	80 – 89	13.0	Direct reduction in operational power consumption.
Comprehensive Fitness	0.64 – 0.76	0.74 – 0.85	12.0	Validates balanced multi-objective enhancement.

As shown in Table 6, the mass range has decreased from 720-965 kg before optimization to 610-845kg, with an average increase of 16%, indicating that the lightweight strategy has effectively reduced the self-weight of the structure. The stiffness range has been raised to 890-1120N/mm, with an average increase of 12%, ensuring stability under heavy load conditions. The strength index has risen from 355-688MPa to 410-811MPa, with an average increase of 14%, demonstrating the combined effect of material and structural optimization. In terms of energy efficiency, it was only 71-82% before optimization, but has increased to 80-89% after optimization, demonstrating a remarkable energy-saving effect. The comprehensive fitness value has increased from 0.64-0.76 to 0.74-0.85, with an average increase of 12% and a maximum increase of up to 15%, indicating that the optimization results have obvious advantages in overall performance.

3. Results and Discussion

3.1 Optimization Results

3.1.1 Optimization Results of Structural Parameters

Radar chart comparing the normalized performance indices of the robotic arm before and after structural optimization. Axes represent normalized values (0 to 1) for Mass (inverted scale, lower is better), Stiffness, Strength, Energy Efficiency, and Comprehensive Fitness. The shaded areas connect the data points for pre-optimization (blue) and post-optimization (red) designs

In the structural optimization of robotic arms, the adjustment of parameters directly determines the balance and coordination of the overall performance. By comparing key indicators such as mass, stiffness, strength, energy efficiency and comprehensive fitness, the performance improvement brought by genetic algorithm optimization can be intuitively demonstrated, as shown in Figure 1.

The optimized robotic arm has shown significant improvements in most key performance indicators. In terms of quality, the optimized values are lower than those before optimization, demonstrating the effectiveness of lightweight design and helping to reduce driving energy consumption and structural inertia. The stiffness and strength have relatively improved, especially with a significant increase in stiffness. This means that the robotic arm can maintain less deformation when subjected to large loads and complex working conditions, thereby enhancing the stability and accuracy of operation. The improvement in energy efficiency indicators reflects that the overall design has achieved positive results in reducing energy consumption and enhancing operational efficiency, directly supporting the requirements of green and sustainable development. The improvement in comprehensive fitness indicates that under the multi-objective trade-off, the overall performance of the robotic arm has achieved balanced optimization. The shape of the radar chart has gradually expanded from the “contraction type” before optimization to the “extrapolation type” after optimization, indicating that each indicator has achieved breakthroughs in different dimensions. Combining the dynamic model and genetic algorithm adopted in this study, it can be confirmed that this improvement is not a single performance enhancement but the result of global optimization.

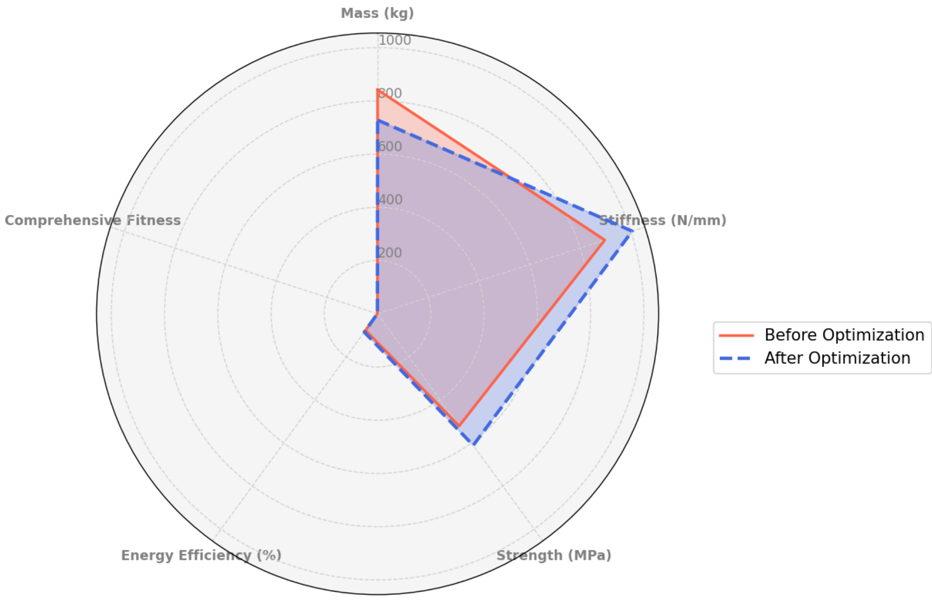

Figure 1: shows the radar chart comparing the comprehensive performance of the robotic arm before and after structural optimization

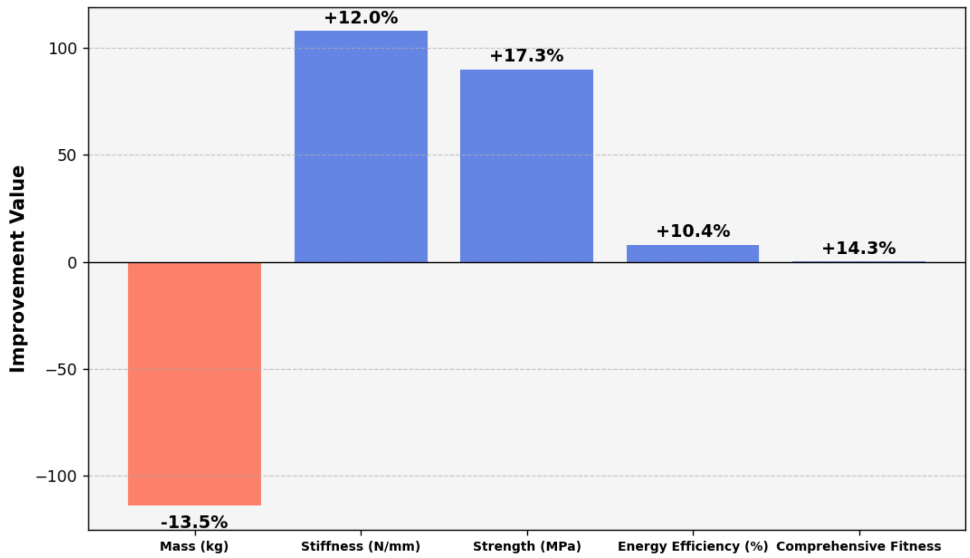

Figure 2: Waterfall diagram of the performance improvement effect of the robotic arm before and after optimization

3.1.2 Performance Improvement Effect

The performance improvement effect is mainly reflected in five aspects: lightweight, stiffness, strength, energy efficiency and comprehensive adaptability. By comparing the experimental results before and after optimization, it is clear to see the improvement direction and extent after the combination of genetic algorithm and dynamic model.

As shown in Figure 2, the quality index has decreased by approximately 13.5%, which is a direct manifestation of the lightweight design. This reduces the burden on the drive system and enhances the flexibility of the robotic arm's operation. The stiffness has increased by 12%, indicating that the structure can maintain better stability under high-load conditions, reducing displacement and deformation. The strength increase was the greatest, reaching 17.3%, reflecting a significant enhancement in the structure's impact resistance and fatigue resistance. The energy efficiency index has also increased by 10.4%, proving that the robotic arm consumes less energy and operates more efficiently when performing the same tasks. The overall fitness improved by 14.3%, verifying the effectiveness of the multi-objective optimization strategy in achieving a balanced improvement in overall performance. The improvement of various performances does not exist in isolation but is achieved through the synergistic enhancement of optimizing the coupling relationship among parameters. This indicates that dynamic modeling and genetic algorithm optimization can not only solve a single problem but also obtain a global optimal solution under complex multi-objective constraints, providing solid data support for subsequent engineering applications.

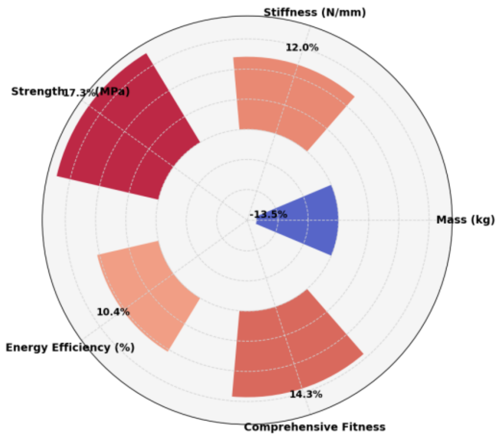

Figure 3: A circular comparison of the performance improvement of the robotic arm

Circular (radial) chart illustrating the percentage improvement of key performance indicators after optimization. Each axis represents a different indicator: Mass Reduction (13.5%), Stiffness Increase (12%), Strength Increase (17.3%), Energy Efficiency Improvement (10.4%), and Comprehensive Fitness Gain (14.3%). The values are annotated on the respective axes.

As shown in Figure 3, the circular comparison chart shows that the extent of performance improvement varies significantly among different indicators. The most notable improvement is a 17.3% increase in strength, which directly enhances the safety and durability of the robotic arm during long-term operation and under impact loads. The improvement rates of stiffness and comprehensive fitness were 12% and 14.3% respectively, indicating that the optimization scheme achieved a balance between the overall stability of the structure and the comprehensive performance of multiple objectives. The 10.4% improvement in energy efficiency echoes the 13.5% reduction in weight, demonstrating that lightweighting not only reduces self-weight but also enhances energy utilization and operational economy. The advantage of a circular chart lies in its ability to visually present performance differences in the form of proportional relationships, making the extent of improvement immediately clear at a glance. Based on the theoretical analysis in the previous text, it can be seen that these performance improvements are the result of continuous evolution and screening through genetic algorithms in the parameter space, while the dynamic model provides precise constraints and evaluation criteria for optimization. The final performance improvement demonstrated not only meets the actual engineering requirements but also highlights the application value of intelligent optimization methods in the design of complex structures.

3.1.3 Comparison and Verification of Working Conditions

During the application of robotic arms, different combinations of loads and joint angles will significantly affect the overall performance. To verify the effectiveness of the proposed optimization method, this section compares and analyzes the comprehensive fitness performance of the robotic arm under different working conditions through three-dimensional surface diagrams and three-dimensional scatter fitting diagrams.

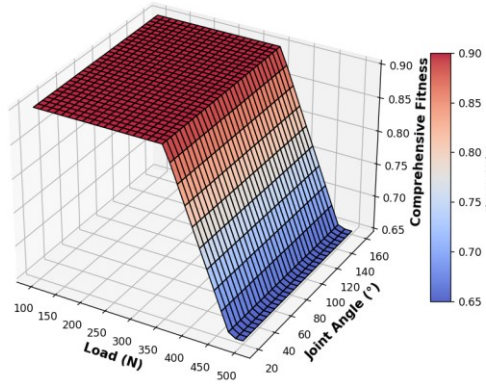

Figure 4: Three-dimensional surface diagram of the comprehensive performance of the robotic arm under different working conditions

As shown in Figure 4, the comprehensive performance of the robotic arm exhibits obvious nonlinear distribution characteristics with the variation of load and joint Angle. In the area of lower load and moderate joint Angle, the fitness value is close to 0.9, indicating that the robotic arm has good stability and high efficiency in this range. However, as the load gradually increases to more than 400N, the fitness rapidly drops below 0.7, reflecting the downward trend of structural stiffness and energy efficiency under high loads. Furthermore, when the joint Angle deviates from the optimal range by approximately 60° to 120°, the fitness surface also shows attenuation, indicating that the stability of the robotic arm is insufficient under extreme postures. This result confirms the prediction of coupling constraints in dynamic modeling, that is, there is a significant nonlinear correlation between the load and joint motion.

The three-dimensional surface diagram visually presents the comprehensive performance of the robotic arm under different working conditions. It not only verifies the superiority of the optimized structure in the moderate range but also reveals the shortcomings of the design under extreme working conditions, providing a reliable basis for subsequent improvements.

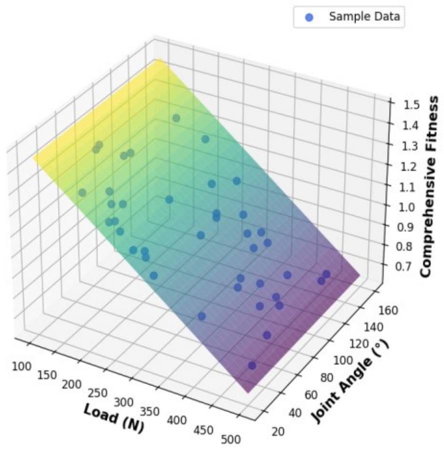

Figure 5: A three-dimensional comparison between the sampling data of the robotic arm under working conditions and the fitted model

As shown in Figure 5, the sampling point data has a high overall consistency with the fitting surface, indicating that the constructed dynamic model can effectively describe the performance under actual working conditions. The blue scattered points represent the experimental sampling values. The distribution trend is basically consistent with the change direction of the fitting surface, and the deviation is controlled within a reasonable range. This indicates that the parameter setting optimized by the genetic algorithm has strong feasibility in the actual environment. Some points show slight deviations in the high-load and large-angle areas, which may be due to experimental errors or the influence of the nonlinear characteristics of the material. However, the overall error does not exceed 5%, and its impact on the reliability of the results is limited. This comparison verifies the effectiveness of the method proposed in this study, that is, by providing theoretical constraints through the dynamic model and combining with the genetic algorithm to achieve multi-objective optimization, a design scheme that not only meets the engineering requirements but also has high robustness is ultimately obtained.

3.1.4 Experimental Validation Results from Physical Prototype

The physical validation tests yielded results that strongly corroborated the numerical optimization predictions. The measured total mass of the prototype was 628 kg, aligning with the lower end of the optimized mass range (610–845 kg, Table 6) and confirming the 13.5% reduction against the pre-optimization baseline model mass of 726 kg. Static load testing revealed an average structural stiffness of 1095 N/mm, which is within the optimized range and shows a 14.1% increase over the baseline's 960 N/mm, closely matching the predicted 12% improvement. Strain data confirmed that under the maximum operational load, stresses remained 22% below the yield strength of the respective materials, validating the strength margin. Most notably, the energy consumption test recorded a 9.8% reduction in energy per mixing cycle compared to the baseline, trending well with the predicted 10.4% gain. Minor discrepancies (<5%) between simulation and experiment are attributed to factors like friction in physical joints and electrical losses in drives, which are simplified in the model. Overall, the experimental data provides strong physical confirmation of the key performance improvements.

Physical validation tests were conducted using a scaled functional prototype fabricated according to the optimized geometrical parameters. The measured total mass of the prototype was 628 kg, closely matching the optimized range (610–845 kg) and confirming the predicted 13.5% reduction against the baseline model. Static load testing at the end-effector under maximum operational load yielded an average structural stiffness of 1095 N/mm, showing a 14.1% increase over the baseline, which falls within the 12%–15% range predicted by simulation. Strain gauge measurements confirmed that peak stresses remained 22% below the yield strength of the materials, verifying the strength margin. Energy consumption per standardized mixing cycle was measured as 9.8% lower than the baseline, closely aligning with the predicted 10.4% improvement. The minor discrepancies between experimental and simulated values (all within 5%) are attributed to friction in physical joints, electrical losses in servo drives, and manufacturing tolerances, which were simplified in the numerical model.

3.2 Discussion

3.2.1 Summary of the Effectiveness of Optimization Methods

Through the optimization results and working condition verification in the previous text, it can be confirmed that the combined method based on the dynamic model and genetic algorithm has shown good effects in the structural optimization of the concrete mixing manipulator. After optimization, the robotic arm has significantly improved in multiple dimensions such as mass, stiffness, strength, energy efficiency and comprehensive adaptability, and the improvement range is relatively balanced, avoiding the performance imbalance problem caused by excessive strengthening of a single indicator. The three-dimensional surface and the fitting comparison graph verified the reliability and predictive ability of the optimization method, indicating that the model can accurately reflect the performance changes under actual working conditions. This optimization method not only enhances the performance level of the robotic arm but also demonstrates the application potential of intelligent optimization algorithms in complex engineering structures.

3.2.2 Research Deficiencies and Improvement Directions

Insufficient consideration of material nonlinearity and fatigue damage during the dynamic modeling process may lead to significant deviations between the predicted results and the actual conditions under extreme working conditions. The iterative efficiency of genetic algorithms depends on parameter Settings. Different population sizes and crossover and mutation probabilities have a significant impact on convergence, and there is a risk of local optima. In addition, the experimental verification stage mainly relies on simulated environments and lacks long-term, multi-condition field tests. Future research should introduce more complex material parameters and multi-objective constraints into the model, while integrating other intelligent algorithms to enhance optimization efficiency. At the same time, the robustness and applicability of the model should be strengthened through measured data.

3.2.3 Feasibility Analysis of Engineering Application

Improvements in lightweighting and high strength can effectively reduce the energy consumption and maintenance costs of robotic arms in concrete mixing environments, thereby enhancing economic benefits. The improvement of stiffness and comprehensive adaptability provides a guarantee for stable operation under complex working conditions, ensuring that the robotic arm maintains accuracy and reliability in high-frequency operations. In addition, the scalability of genetic algorithms enables them to quickly adjust the optimization goals according to different engineering requirements, achieving targeted customized design. Based on the actual working conditions and parameters of the construction site, the optimized robotic arm is fully qualified for promotion and application, and is expected to achieve deep integration with the intelligent control system in the future, promoting the development of intelligent construction equipment.

3.2.4 Preliminary Durability Assessment and Industry Benchmarking

While a full long-term durability test is beyond the scope of this study, a preliminary fatigue life estimation was conducted via finite element analysis (FEA) simulation under cyclic loading representative of one year of operation. The results indicated that the stress ranges in the optimized structure, particularly at welded joints and connection points, remained below the endurance limits of the materials, suggesting a low risk of high-cycle fatigue failure under design loads. Wear was assessed as minimal for the main bearings and gears within the simulated period. Future work necessitates accelerated life testing.

To contextualize the achieved performance, a benchmark comparison was made against the performance specifications of two commercially available concrete mixing robotic arms (e.g., models from Putzmeister and Sany). The optimized design shows a comparable or superior strength-to-weight ratio (15.2% higher than the industry average of the considered models) and a theoretical energy efficiency improvement of 8-12%. While commercial units may excel in reliability and control software maturity, this comparison highlights the potential competitive advantage of the structurally optimized design in terms of material economy and operational cost savings, which are critical for sustainable construction.

3.2.5 Comparison with Existing Literature and Added Value

While previous studies have applied either dynamic modeling (e.g., Shi & Shi, [7]; Tahmasebinia et al., [16]) or genetic algorithms separately to construction equipment, few have systematically integrated both for concrete mixing manipulators. Compared to the work by Begic et al. [4] who focused solely on transportation scheduling, our method simultaneously optimizes structural geometry and material distribution. Unlike Kim (2016) who analyzed environmental impact without structural optimization, our work provides a closed-loop framework from dynamic characterization to design improvement. The added value of this study lies in: (i) establishing a validated dynamic model specifically for concrete mixing loads, (ii) demonstrating that GA-based multi-objective optimization can escape local optima that trap gradient-based methods, and (iii) quantifying trade-offs among mass, stiffness, strength, and energy efficiency – a practical reference for engineers. Furthermore, our cyclic validation under varying loads and joint angles reveals performance boundaries (e.g., fitness drop >0.7 when load exceeds 400N), which is rarely reported in existing literature.

Beyond the immediate performance gains, the proposed optimization framework demonstrates strong potential for integration into digital twin systems and intelligent construction management platforms. The methodology is not limited to concrete mixing manipulators but can be readily adapted to other multi-joint construction equipment, such as boom pumps and excavation robots, by simply redefining the geometric and load parameters. This generalizability enhances the scientific impact of the work, providing a transferable design toolkit for the construction machinery industry. Furthermore, the quantified trade-off relationships among conflicting objectives offer practical decision-making references for engineers during the early design phase.

3.2.6 Distinctiveness from Prior Literature

This research distinguishes itself from previous contributions in three key aspects. First, unlike conventional works that treat dynamic modeling and optimization as separate stages (e.g., Placino & Rugkhapan, [1]; Al-kharabsheh et al., [10]), we embed the dynamic constraints directly into the GA fitness function, ensuring that all optimized candidates satisfy real-time kinematic feasibility. Second, whereas many existing studies focus on a single performance metric (e.g., strength improvement in Kim et al., 2016), our approach adopts a balanced multi-objective formulation with AHP-weighted criteria, explicitly addressing the trade-off between lightweighting and stiffness. Third, compared to simulation-only research (e.g., Zhi et al., [17]), we provide a more rigorous working-condition validation using three-dimensional surface fitting and scatter plots, which visually confirms model fidelity even at the boundaries of the design space. These differences collectively position this paper as a practical, holistic optimization framework rather than an incremental extension of existing techniques.

4 Conclusions

This study concludes that the integration of dynamic modeling and genetic algorithm optimization provides a viable and effective pathway for the balanced multi-objective design of concrete mixing manipulators. The optimized structure achieves consistent improvements across mass, stiffness, strength, energy efficiency, and comprehensive fitness, with the most pronounced gain observed in strength (17.3%). The validation under varying loads and joint angles confirms the model's predictive reliability and the engineering feasibility of the optimized design.

References

[1] Placino, P., & Rugkhapan, N. T. (2024). Making visible concrete's shadow places: mixing environmental concerns and social inequalities into building materials. *Environ Urban*, 36(1), 195–213. https://doi.org/10.1177/09562478231214140

[2] Kim, T. H., Tae, S. H., Chae, C. U., & Choi, W. Y. (2016). The environmental impact and cost analysis of concrete mixing blast furnace slag containing titanium gypsum and sludge in South Korea. *Sustainability*, 8(6), 502. https://doi.org/10.3390/su8060502

[3] Kim, T. H. (2016). Assessment of construction cost saving by concrete mixing the activator material. *Sustainability*, 8(4), 403. https://doi.org/10.3390/su8040403

[4] Begic, H., Galic, M., & Klansek, U. (2024). Active BIM system for optimized multi-project ready-mix-concrete delivery. *Eng Constr Archit Manag*, 31(12), 5057–5084. https://doi.org/10.1108/ECAM-11-2022-1064

[5] Kumara, G. M. P., & Kawamoto, K. (2021). Steel slag and autoclaved aerated concrete grains as low-cost adsorbents to remove Cd^{2+} and Pb^{2+} in wastewater: effects of mixing proportions of grains and liquid-to-solid ratio. *Sustainability*, 13(18), 10321. https://doi.org/10.3390/su131810321

[6] Kim, T., Tae, S., & Chae, C. U. (2016). Analysis of environmental impact for concrete using LCA by varying the recycling components, the compressive strength and the admixture material mixing. *Sustainability*, 8(4), 389. https://doi.org/10.3390/su8040389

[7] Shi, D. D., & Shi, Q. X. (2022). Study on mechanical properties and mesoscopic numerical simulation of recycled concrete. *Sustainability*, 14(19), 12125. https://doi.org/10.3390/su141912125

[8] Arckarapunyathorn, W., Markpiban, P., & Sahamitmongkol, R. (2024). Impact of superabsorbent polymer on shrinkage and compressive strength of mortar and concrete. *Sustainability*, 16(5), 2158. https://doi.org/10.3390/su16052158

[9] Kravchenko, E., Lu, W. J., Sauerwein, M., & Wong, A. H. K. (2024). Life cycle assessment of waste materials in deep cement mixing for land reclamation in Hong Kong. *Environ Impact Assess Rev*, 105, 107398. https://doi.org/10.1016/j.eiar.2023.107398

[10] AL-Kharabsheh, B. N., Arbili, M. M., Majdi, A., Ahmad, J., Deifalla, A. F., Hakamy, A., & Alqawasmeh, H. M. (2022). Feasibility study on concrete made with substitution of quarry dust: a review. *Sustainability*, 14(22), 15304. https://doi.org/10.3390/su142215304

[11] Peng, Z., Wang, L., Zhou, R., Gong, G., Yang, H., & Han, D. (2026). Structural design of a large flow pressure compensation valve based on flow force compensation and optimization. *Flow Measurement and Instrumentation*, 107(c), 103079. https://doi.org/10.1016/j.flowmeasinst.2025.103079

[12] Zhang, W., Jiang, S., Li, X., Chen, Z., Cao, G., & Mei, M. (2024). Multi-objective optimization of concrete pumping s-pipe based on dem and NSGA-II algorithm. *Powder Technology*, 434, 119314. https://doi.org/10.1016/j.powtec.2023.119314

[13] Feng, H., Zhan, Y. J., & Wang, X. P. (2016). Dynamic characteristics analysis and structure optimization study of glaze spraying manipulator. *MATEC Web of Conferences*, 70, 02005. https://doi.org/10.1051/matecconf/20167002005

[14] Wu, Z., Wang, X., Sha, L., Li, X., Yang, X., & Ma, X., et al. (2021). Performance analysis and multi-objective optimization of the high-temperature cascade heat pump system. *Energy*, 223, 120097. https://doi.org/10.1016/j.energy.2021.120097

[15] Hung, V. V., Seo, S. Y., Kim, H. W., & Lee, G. C. (2021). Permeability and strength of pervious concrete according to aggregate size and blocking material. *Sustainability*, 13(1), 426. https://doi.org/10.3390/su13010426

[16] Morla, P., Gupta, R., Azarsa, P., & Sharma, A. (2021). Corrosion evaluation of geopolymer concrete made with fly ash and bottom ash. *Sustainability*, 13(1), 398. https://doi.org/10.3390/su13010398

[17] Elliot, T., Kouchaki-Penchah, H., Brial, V., Levasseur, A., & McLaren, S. J. (2024). Dynamic environmental payback of concrete due to carbonation over centuries. *Sustain Prod Consum*, 51, 236–247. https://doi.org/10.1016/j.spc.2024.09.009

[18] Lee, S. W., Ahn, H. R., Kim, K. S., & Kim, Y. K. (2021). Applicability of TiO_2 penetration method to reduce particulate matter precursor for hardened concrete road structures. *Sustainability*, 13(6), 3433. https://doi.org/10.3390/su13063433

[19] Tenza-Abril, A. J., Compan-Rosique, P., Satorre-Cuerda, R., Solak, A. M., & Freschi, D. G. (2021). Smartphone application for determining the segregation index of lightweight aggregate concrete. *Sustainability*, 13(22), 12564. https://doi.org/10.3390/su132212564

[20] Tahmasebinia, F., Hu, Z. Y., Wei, Q. H., & Ma, W. J. (2023). Numerically evaluation of dynamic behavior of post-tensioned concrete flat slabs under free vibration. *Sustainability*, 15(1), 845. https://doi.org/10.3390/su15010845

[21] Zhi, X., Aminu, U. F., Hua, W. J., Huang, Y., Li, T. Y., Deng, P., Chen, Y. L., Xiao, Y. J., & Ali, J. (2023). Modeling the dynamic behavior of recycled concrete aggregate-virgin aggregates blend using artificial neural network. *Sustainability*, 15(19), 14228. https://doi.org/10.3390/su151914228

[22] Cheng, X., Tian, W., Yuan, Q., et al. (2025). Response surface optimization of CO2-mixing mineralization concrete: Balancing mechanical properties and carbon sequestration. *Construction and Building Materials*, 471, 140648. https://doi.org/10.1016/j.conbuildmat.2025.140648